

Evolution of mechanical properties and corrosion resistance of Al-Zn-Mg alloy with different numbers of flame rectification at 350°C

ABSTRACT

This paper investigated the microstructure, tensile properties, intergranular corrosion resistance and exfoliation corrosion resistance of Al-4.5Zn-1.5Mg (wt.%) alloy after undergoing different numbers of flame rectification at 350°C. The results showed that the flame rectification accelerated the corrosion susceptibility of Al-Zn-Mg alloy. And the maximum intergranular corrosion depth are detected with the value of 105µm after one time of flame rectification. The tensile strength of Al-Zn-Mg alloy decreased to 317 MPa after one time of flame rectification, but increased to 387 MPa after two times of flame rectification in 350 °C. The change of corrosion resistance of Al-Zn-Mg alloy with varied flame rectifications is mainly associated with the transformation of precipitates and grains. After one time of flame rectification, a phenomenon of "redissolution" of precipitated phases occurs. However, there is a notable increase in the precipitation of phases within the grains after two and three times of flame rectification at 350°C. After one time of flame rectification, small-sized new grains appear at the grain boundaries of the elongated grains within the correction area, which is the result of incomplete recrystallization in the alloy.

Keywords: Al-Zn-Mg alloy; flame rectification; microstructure; mechanical properties; corrosion properties.

1. INTRODUCTION

Al-Zn-Mg alloys are widely used because of their high specific strength, hardness, good weldability and corrosion resistance. However, the difficulty in controlling residual stress and deformation of Al-Zn-Mg alloys has become a major challenge. To solve this challenge, flame rectification (FR) is a great method^[1]. Due to the uneven heating and cooling of the welding process, welding deformation of Al alloy workpieces is inevitable. Currently, there are three categories of measures available to control welding distortion: 1. Before welding, during the design stage of welding structure, welding deformations can be predicted using computational methods (such as numerical simulation techniques). Subsequently, measures such as optimizing structural design and positioning weld seams reasonably can be employed to "proactively" control welding deformations. 2. During welding, in the stage of welding manufacturing (assembly), "proactive" control of welding deformations can be achieved by controlling heat input, optimizing welding sequences, and utilizing external constraints and counter-deformation measures. 3. Post-weld heat treatment (thermal correction or mechanical correction), which falls under the category of "passive" control methods, which may increase costs and energy consumption^[2,3]. If welding distortion cannot be controlled within the allowable range by using pre-welding and during-welding straightening methods, it is necessary to carry out post-welding correction.

The methods of post-weld straightening include mechanical straightening method (cold straightening) and FR method (heat straightening)^[4,5]. Mechanical straightening is the use of mechanical methods such as hammering, presses and other mechanical methods to counteract welding distortion of structural components by inducing plastic deformation in the weld material. The FR is based on the characteristics of heat expands and cold contracts of metal materials. In the welding distortion area after heating and cooling, so that the welded structural components to produce anti-deformation, to achieve the purpose of correcting the welding distortion^[6,7]. Mechanical straightening is generally suitable for small parts, whereas

FR is primarily appropriate for larger parts. FR can be divided into three types for heating purposes: point heating, line heating and triangular heating, as shown in Fig. 1. Fig. 2 shows a schematic diagram of the principle of triangular thermal correction. The FR is typically heated by an oxygen-acetylene flame, with a maximum temperature of approximately 3200°C. By moving the oxyacetylene flame, the distortion area is heated and then quenching in water immediately, which in turn reduces the welding distortion. The FR is widely used in the production of straightening of welding distortion of structural parts of iron and steel materials due to the advantages of easy operation and flexibility [8,9]. With the continuous expansion of the application scope of high-strength Al alloy in the field of equipment manufacturing. The Al alloy FR process and its impact on the structure properties of components is gradually attracting extensive attention from researchers.

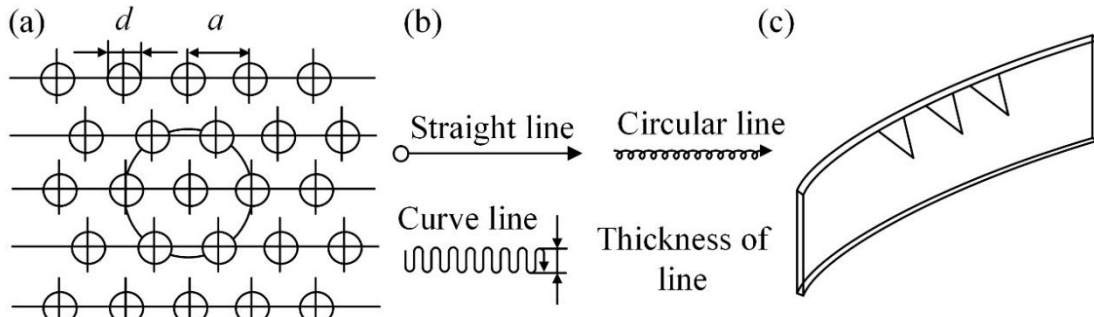


Fig. 1. The common heating methods for FR (a) spot heating; (b) linear heating; (c) triangle heating.

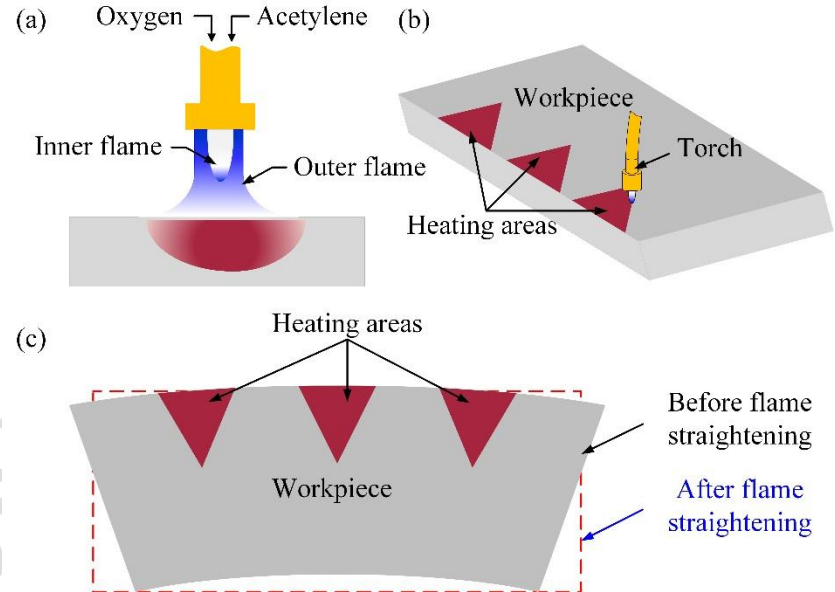


Fig. 2. The schematic diagram of heat straightening flame heating; (b) heat areas; (c) before and after FR.

Jiang [9] used flame heating to correct the welding distortion of 7020 Al alloy. The findings demonstrate that the mechanical properties of the welded joints remain unchanged at a correction temperature of 125°C. However, at temperatures above 225°C, there is a gradual increase in the tensile strength of the joints with an increase in correction temperature. Additionally, when the straightening temperature reaches above 325°C, the softening zone becomes wider, and the hardness reduces gradually with an increase in straightening temperature. Therefore, it is recommended that the correction of 7020 Al alloy

should be carried out below 325°C. Temperature field tests have shown that FR creates an unstable instantaneous temperature field that is vulnerable to operational factors ^[10]. Moreover, Avent ^[11-13] stressed that "the process remains more of an art than a science". Thus, it is evident that the use of flame heating method cannot precisely analyze the causes of the alteration in alloy performance. To better investigate the influence of heat treatment parameters on the microstructure and properties of 7N01 Al alloy. Xiong ^[10] conducted a study on the impact of FR temperature on the microstructure as well as mechanical properties of Al alloy joints in high-speed trains, using Gleeble thermal simulation testing machine. The study revealed that the FR temperature did not significantly alter the hardness of the weld zone. However, the hardness of the 7N01 Al alloy base metal and the heat-affected zone decreased when the temperature was below 300°C, whereas it increased between 300-350°C. Therefore, the recommended heat correction temperature for 7N01 Al alloy is between 300-400°C.

2. MATERIALS AND METHODS

2.1 MATERIALS AND FLAME CONDITIONING METHODS

The experimental material in this paper is Al4.5Zn1.5Mg-T5 profile. The material size is 5mm×40mm×140mm and the base metal composition are shown in Table 1.

Table 1 Chemical composition of base metals and filler metal (wt.%)

Materials	Zn	Mg	Mn	Cr	Zr	Fe	Cu	Ti	Si	Al
Al4.5Zn1.5Mg-T5	4.48	1.55	0.29	0.23	0.18	0.13	0.11	0.05	0.05	Bal

During the FR, combustible mixed gases, including oxygen-acetylene flame, are employed to heat the corrective area. The flame heating process generates a local transient temperature field, which varies with heating time and location. Furthermore, it is influenced by operational factors, can not obtain a stable temperature field, which hinders precise control of the corrective temperature. To better investigate the effects of FR parameters on the phase transformation and corrosion performance of Al4.5Zn1.5Mg-T5 alloy, reduce the influence of other factors on experimental results, and make the experimental conclusions more convincing. In this paper, the effect of FR parameters on the mechanical and corrosion properties of Al-Zn-Mg alloys is investigated by means of FR, and the specimen numbers are shown in Table 2.

Table 2 The serial number of Al4.5Zn1.5Mg-T5 alloy samples under different heat straightening numbers

Samples No.	Number of times in heat treatment	Temperature (°C)	Heating time (s)
BM	-	-	-
WQ1	1	350	120
WQ2	2	350	120
WQ3	3	350	120

2.2 MICROSTRUCTURE OBSERVATION AND ANALYSIS

The treated specimens were coarsely ground and finely ground to 2000 grit size with SiC sandpaper. Polishing with diamond abrasive paste with a grain size of 1.5 μm. After polishing was completed, the corrosion was carried out with mixed acid (2 mL HF + 3 mL HCl + 5 mL HNO₃ + 190 mL H₂O), and the corrosion time was about 45 s. Immediately after corrosion, rinse with clean water and dry with a hair dryer. The metallographic structure of Al-Zn-Mg alloy matrix was observed by Leica MEF4 metallographic microscope.

The microstructures of the alloys and welded joints were observed and analyzed using a Zeiss supra55 Field Emission Scanning Electron Microscope (SEM) with Energy Dispersive

Spectroscopy (EDS). SEM second electron images were used to analyze fracture of room temperature tensile and slow strain rate tensile specimens under different heat treatment conditions to determine the fracture mechanism. It can also be used to observe local corrosion morphology and compositional analysis.

The specimens were analyzed using the Electron Backscattered Diffraction (EBSD) analysis function attached to the SEM. EBSD samples underwent coarse grinding, fine grinding, and mechanical polishing, then they were subjected to electrolytic polishing to remove surface stress. The electrolyte solution consists of 30% nitric acid and 70% methanol (by volume at a temperature of -30°C). For electrolytic polishing, the voltage was set at 15 V, and the electrolytic polishing time ranged from 10 to 20 seconds. After electropolishing, the sample is cleaned in alcohol to remove residual corrosive liquid, then it is rinsed using an ultrasonic cleaning machine. Afterwards, sample is removed and dried with a hair dryer before further processing. For EBSD observation, the applied voltage is 20 kV, and the step size is $1.5\ \mu\text{m}$.

2.3 MECHANICAL PROPERTIES TEST AT ROOM TEMPERATURE

The tensile test samples at room temperature were prepared according to the standard GB/T 228.1-2010. The test equipment was DNS100 universal tensile testing machine, with a tensile rate of 5 mm/min, and each measured value was the average of three sets of parallel samples. Thermal cycling tensile specimens using the dimensions shown in Fig. 3.

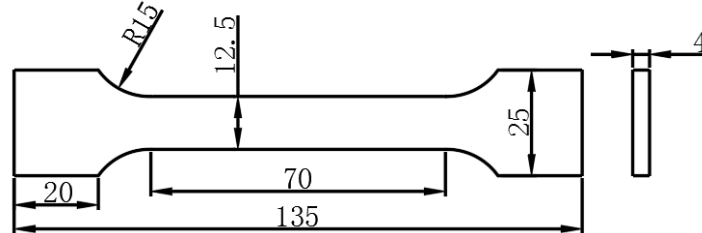


Fig. 3. Dimensions of repetitious heat straightening samples for tensile test (Unit, mm)

2.4 CORROSION PERFORMANCE TEST

The intergranular corrosion test was conducted according to the standard ASTM G110-92 and the samples with dimensions of $40\ \text{mm} \times 25\ \text{mm} \times 5\ \text{mm}$ were extracted from the samples after FR for intergranular corrosion (IGC) test^[14]. Before the experiment, polish the samples with SiC sandpaper up to 1200 grit, and rinse them with acetone to remove surface oil contaminants. The sample was immersed in a 10 wt.% NaOH solution for 5-15 minutes, then removed and rinsed with deionized water. Subsequently placed in 30 vol.% HNO_3 solution until the surface of the specimen is bright. Rinse with deionized water and dry with a hair dryer. The non-working surface of the specimen was sealed with epoxy AB glue. The intergranular corrosion solution was composed of 57g of pure NaCl and 10mL of pure H_2O_2 , which were diluted to 1L with deionized water. Maintain the soaking temperature within the range of $35 \pm 2\ ^{\circ}\text{C}$ using a thermostatic water bath. After completing the intergranular corrosion test, the specimen was mechanically cut 5 mm from the specimen in the direction of the perpendicular main deformation. Then embed the sample for grinding and polishing, then use an optical microscope (OM) to observe and measure the corrosion depth.

The exfoliation corrosion (EXCO) test was conducted according to the standard ASTM G34-01^[15]. The specimens were prepared as follows: sandpaper sanding \rightarrow acetone cleaning \rightarrow deionized water cleaning \rightarrow blow-drying. The corrosion solution composition is: 4 M NaCl + 0.5 M KNO_3 + 0.1 M HNO_3 , the pH value of the solution is about 0.4, and the temperature of the corrosion solution is maintained at $25 \pm 2\ ^{\circ}\text{C}$. The specimen is immersed in a corrosive solution and removed at regular intervals. The macroscopic corrosion morphology of the specimen surface was recorded with a camera, and the exfoliation corrosion grade was assessed with a total immersion time of 48 h.

3. EXPERIMENTAL RESULTS AND ANALYSIS

3.1 COMPARATIVE ANALYSIS OF MICROSTRUCTURE

The microstructure of Al-4.5Zn-1.5Mg (wt.%) alloy in the straightening area at 350°C with different numbers of FR is shown in Fig. 4. As can be seen from the figure, the Al-4.5Zn-1.5Mg (wt.%) alloy in the unstraightened and 350°C-FR areas consists of a large number of elongated grains distributed along the extrusion direction, and there is no obvious recrystallization. A large number of fine and diffuse MgZn₂ precipitation phases are distributed both in the grain and at the grain boundaries, in addition to a small number of large-sized massive precipitation phases α -AlFeMnSi. Compared with the unstraightened area, the number of intracrystalline precipitates was slightly reduced after the first 350°C-flame straightening, there was a tendency to dissolve into the matrix, and the grains grew significantly.

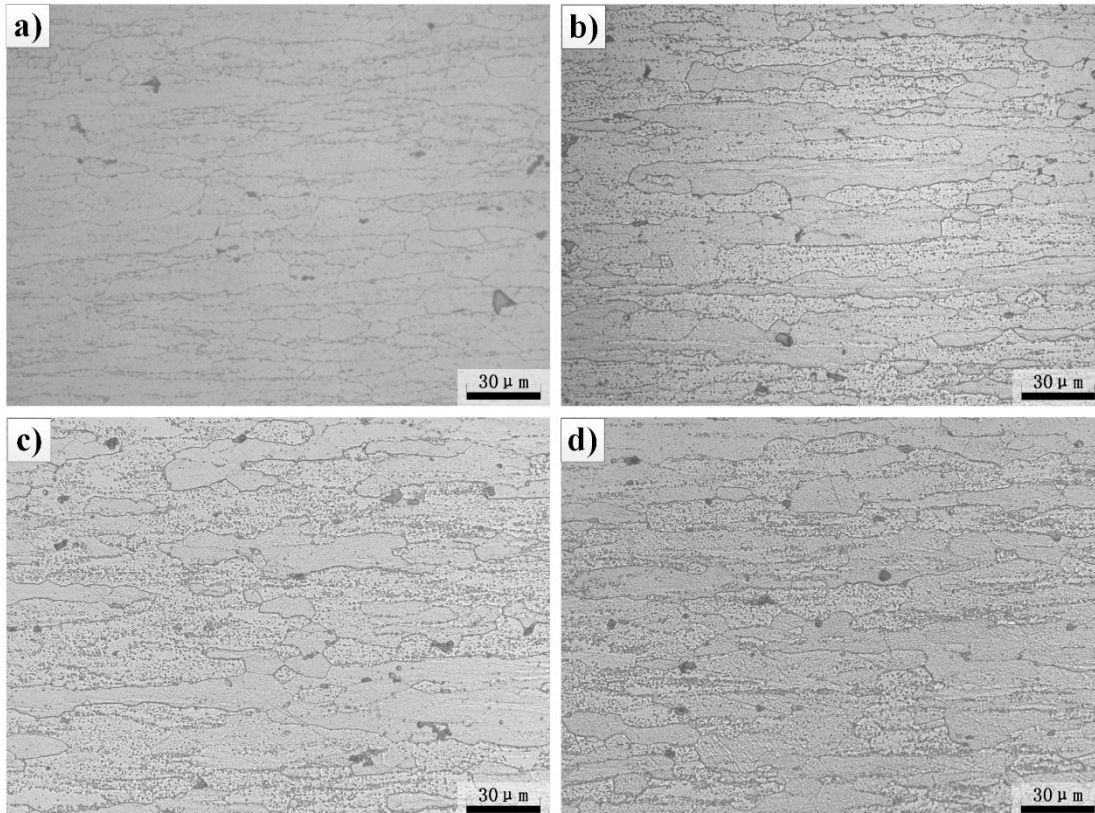


Fig. 4. Microstructure of Al-4.5Zn-1.5Mg (wt.%) alloy inside the region of flame rectification after different numbers of FR in 350°C (a) base metal, (b) one time, (c) two times (d) three times

3.2 COMPARATIVE ANALYSIS OF MECHANICAL PROPERTIES

Fig. 5 shows the variation of mechanical properties within the straightening area for Al-4.5Zn-1.5Mg (wt.%) alloy at 350°C with different FR numbers of FR conditioning. From the figure, it can be observed that after a single FR at 350°C, the tensile strength of the alloy significantly decreases. However, after the second and third FR, the strength rises again and is noticeably higher than the value before straightening. The trend of elongation was similar to that of tensile strength. That is, it drops sharply after one straightening, picks up quickly after the second straightening, and then drops to values close to those of the parent material after the third straightening.

The mechanical properties of materials are closely related to the microstructure. The strength of Al-Zn-Mg alloys mainly comes from the strengthening of precipitates. The

decrease in the density of precipitates and grain growth combined to cause a significant decrease in the tensile strength of the Al-4.5Zn-1.5Mg (wt.%) alloy after a single 350°C-FR. After the second and third straightening, the precipitates increase and produce a strengthening effect, so the tensile strength of the alloy rises and exceeds that of the untreated alloy. As the microstructure is similar after the second and third straightening, the tensile strength values are also close to each other.

The morphology of the tensile fracture in the area of straightening at 350°C with different number of FRs is shown in Fig. 6. As can be seen from the figure, the Al-4.5Zn-1.5Mg (wt.%) alloy has relatively good plasticity before and after FR in 350°C. The presence of dimples of different sizes on the fracture is typical of ductile fracture. Comparing the microscopic fracture morphology in the area of untreated and 350°C-FR, it can be found that the dimples on the fracture after the primary rectification are smaller in size and shallower in depth relative to those in the untreated area, which indicates that the plasticity is poor. After the second straightening, the dimples become larger and deeper, and the plasticity is improved. After the third straightening, the depth of the dimples becomes shallow, and the plasticity decreases. The plasticity trend reflected in the dimples is consistent with the trend of the extension first decreasing and then increasing, and finally decreasing to close to the parent material in Fig. 5.

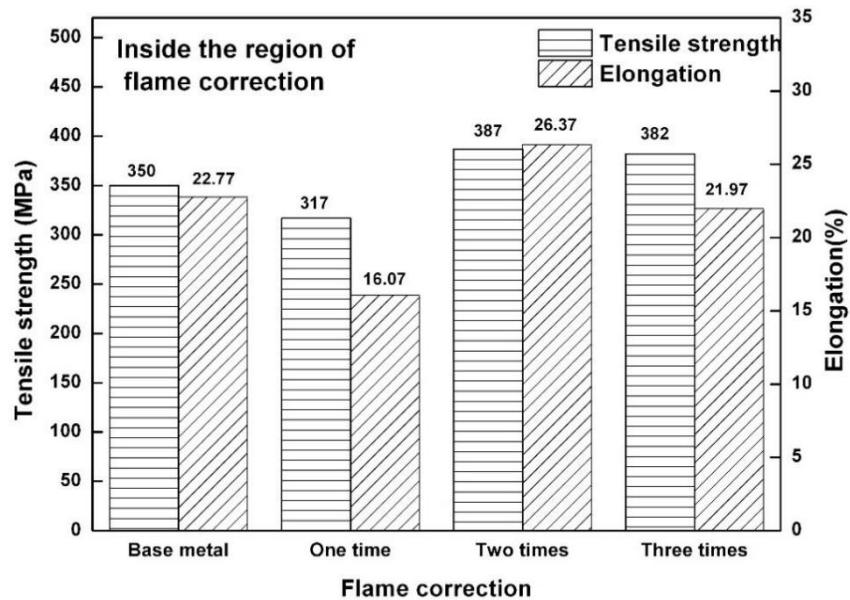


Fig. 5. Tensile strength and elongation of Al-4.5Zn-1.5Mg(wt.%) alloy inside the area of flame rectification Vs. times of FR in 350°C

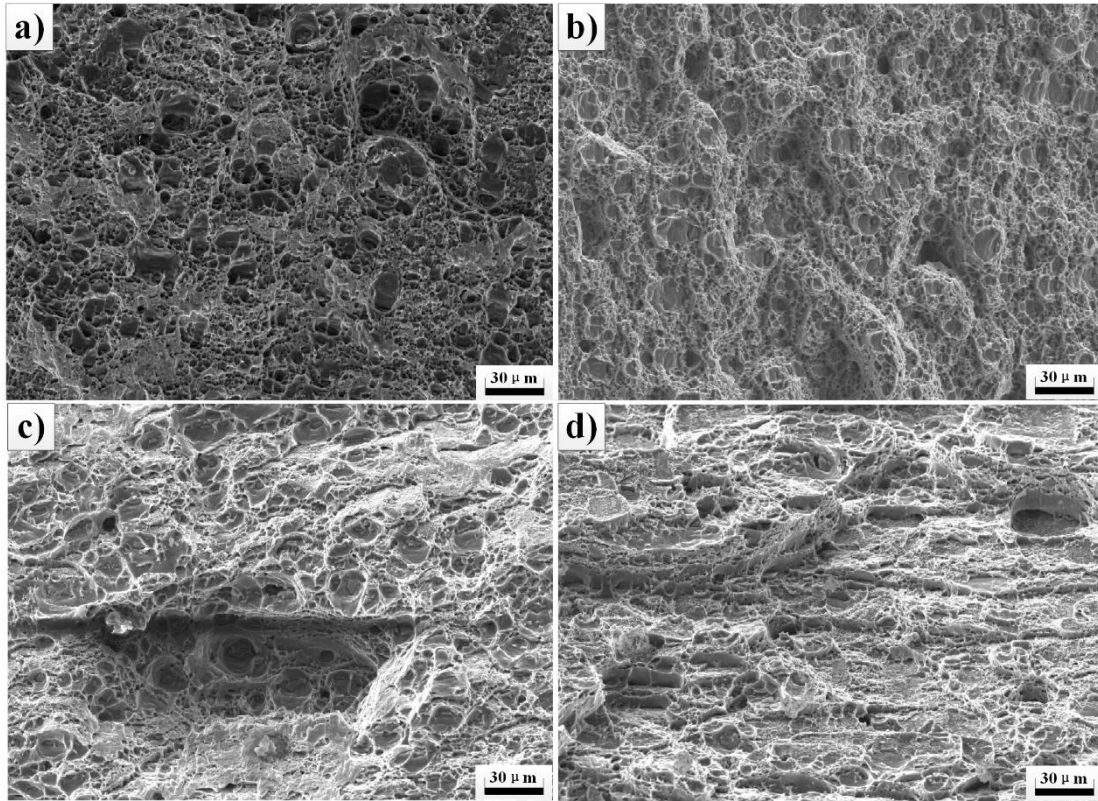


Fig. 6. SEM images of the tensile fractures of Al-4.5Zn-1.5Mg(wt.%) alloy inside the area of flame rectification after different numbers of FR in 350°C (a) base metal, (b) one time, (c) two times (d) three times

The variation of mechanical properties of Al-4.5Zn-1.5Mg (wt.%) alloy outside the straightening area at 350°C with different number of FR is shown in Fig. 7. From the figure, it can be observed that the tensile strengths of the alloys outside the straightening area were all increased after FR in 350°C. This result may be related to the fact that the alloys outside the straightening area were partially recrystallized after FR in 350°C and the values of the tensile strengths did not differ much after the straightening. The elongation shows an opposite trend to the tensile strength, with an overall decrease. After the 350°C-FR, the trends of tensile strength and elongation inside and outside the straightening area differ greatly. This is due to the fact that the inside of the straightening area is more affected by the circulating heat of the flame. The outside of the straightening area is far away from the flame, less affected by the heat, and has a slow rate of warming. So that the temperature and the amount of heat outside of the straightening area are not able to reach the values inside the straightening area, and therefore show different trends.

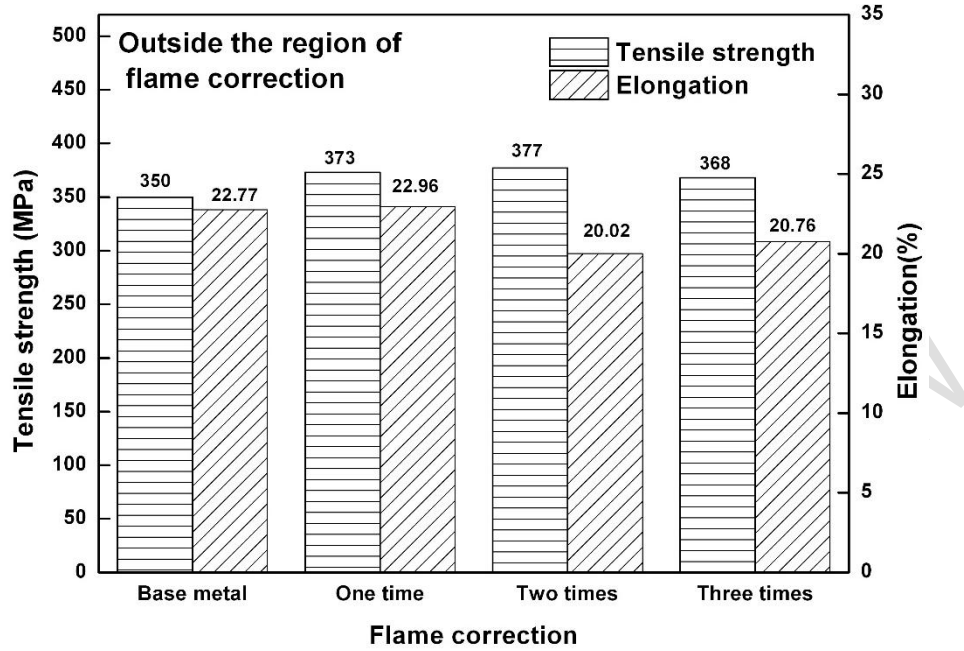


Fig. 7. Tensile strength and elongation of Al-4.5Zn-1.5Mg(wt.%) alloy outside the area of flame rectification Vs. times of FR in 350°C

The tensile fracture morphology of Al-4.5Zn-1.5Mg (wt.%) alloy outside the straightening area at 350°C with different FR times is shown in Fig. 8. As can be seen from the figure, the alloys outside the straightening area also exhibit tough fracture characteristics, and there are many dimples of different sizes on the fracture. The dimples on the fracture of unstraightened and the 350°C-FR alloys are of comparable sizes, indicating similar plasticity. After the second and third straightening, the dimples decrease in size and the plasticity decreases. This trend is consistent with the extended first slight increase and then decrease in Figure 7.

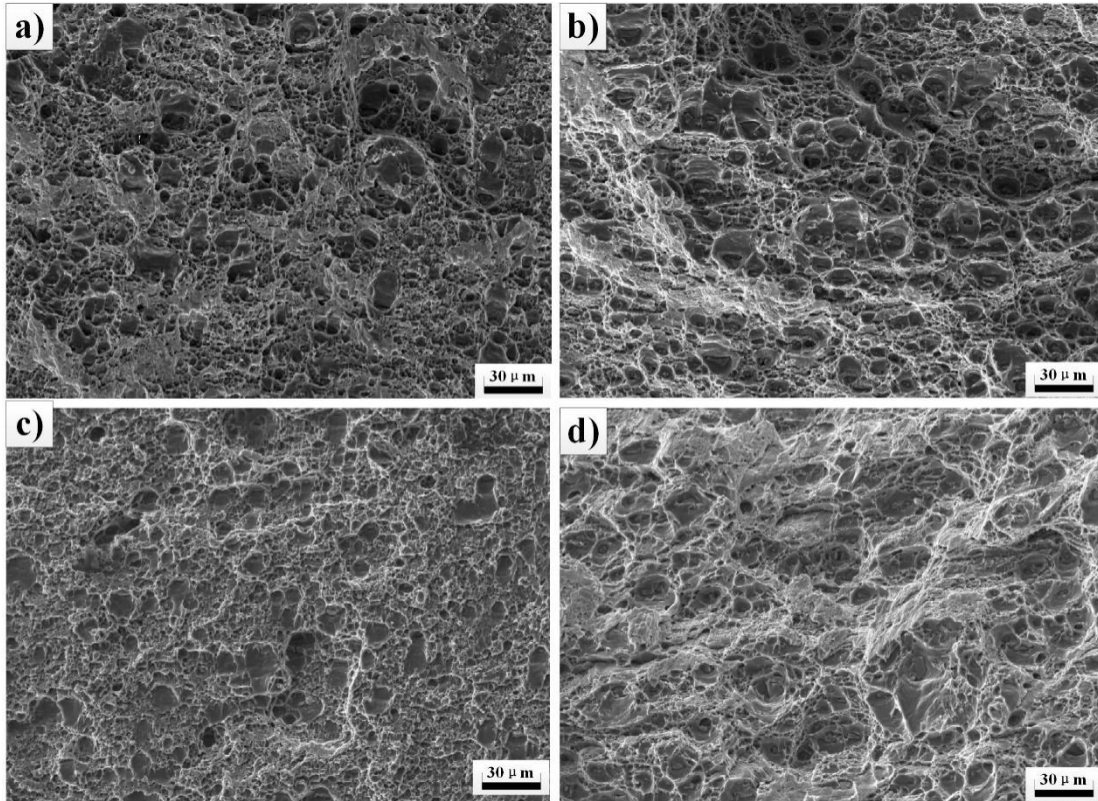


Fig. 8. SEM images of the tensile fractures of Al-4.5Zn-1.5Mg(wt.%) alloy outside the area of flame rectification after different numbers of FR in 350°C (a) base metal, (b) one time, (c) two times (d) three times

3.3 COMPARATIVE ANALYSIS OF CORROSION PERFORMANCE

The intergranular corrosion morphology of Al-4.5Zn-1.5Mg (wt.%) alloy in the straightening area at different FR times in 350°C is shown in Fig. 9. As can be seen from the figure, after 350°C-FR, localized reticulated grain boundaries appeared in each specimen, i.e., intergranular corrosion occurred to different degrees. Comparison of the intergranular corrosion morphology after the first, second and third straightening can be found, the 350°C-FR after the first specimen corrosion is the most serious. After the first, second and third straightening, the maximum depth of intergranular corrosion of the specimen were 0.105mm, 0.080mm, 0.076mm, according to GB/T7998-2005, the corresponding corrosion grade were 2, 3, 3. However, intergranular corrosion was still not observed in specimens outside the straightening area. Intergranular corrosion is mainly related to the formation of primary batteries between grains and grain boundaries^[16].

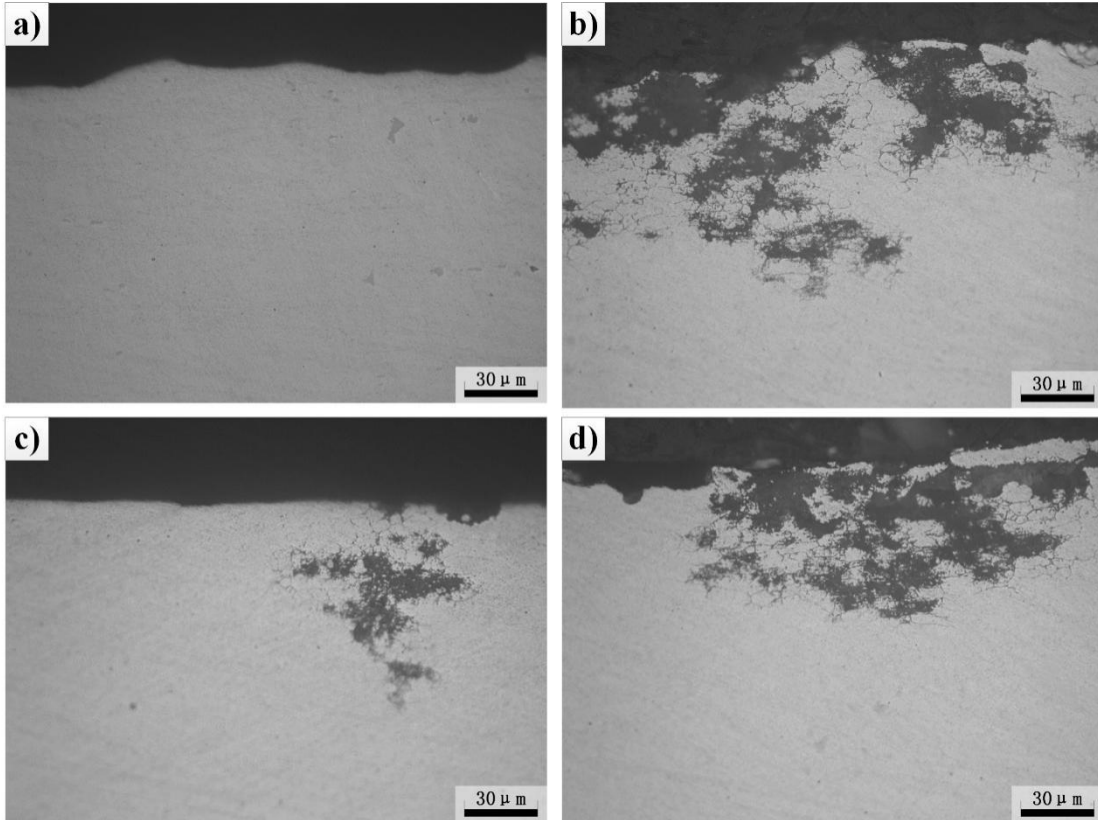


Fig. 9. Intergranular corrosion micrographs of Al-4.5Zn-1.5Mg(wt.%) alloy inside the area of flame rectification after different numbers of FR in 350°C (a) base metal, (b) one time, (c) two times (d) three times

The macroscopic morphology of exfoliation corrosion of Al-4.5Zn-1.5Mg (wt.%) alloy in the straightening area under different FR times at 350°C is shown in Fig. 10. As can be seen from the figure, after the 350°C-FR, the whole surface of the specimen in the straightening area showed uniform and severe exfoliation corrosion. The metal surface was uneven and delamination phenomenon, and the test solution after corrosion contained a large number of exfoliation products. The difference between the right side of the specimen in Fig. 10(d) and the overall corrosion degree may be due to the sampling process is not standardized, so that the right side is taken outside the straightening area caused.

A partially exfoliated specimen was intercepted observed under the scanning electron-microscope, and the results are shown in Fig.11. From the figures, it can be observed that, the surface of the specimen before and after FR along the crystal cracking phenomenon, and produce layer separation. Comparison of the microscopic corrosion morphology after 350°C-FR in the first, second and third straightening reveals that the stripping phenomenon is the most serious in the area of 350°C FR in the first straightening. The specimen surface appeared obvious along the crystalline cracks, and has been deep into the metal inside quite deep. After the 350°C-FR two or three times the corrosion degree of the specimen is not much different. Three times the specimen is slightly more serious than the second rectification specimen, along the crystal cracks slightly wider. According to GB/T22639-2008, the exfoliation corrosion level of the specimens in the area of the straightening after 350°C-FR of Al-4.5Zn-1.5Mg (wt.%) alloy in the first, second and third time is ED level.

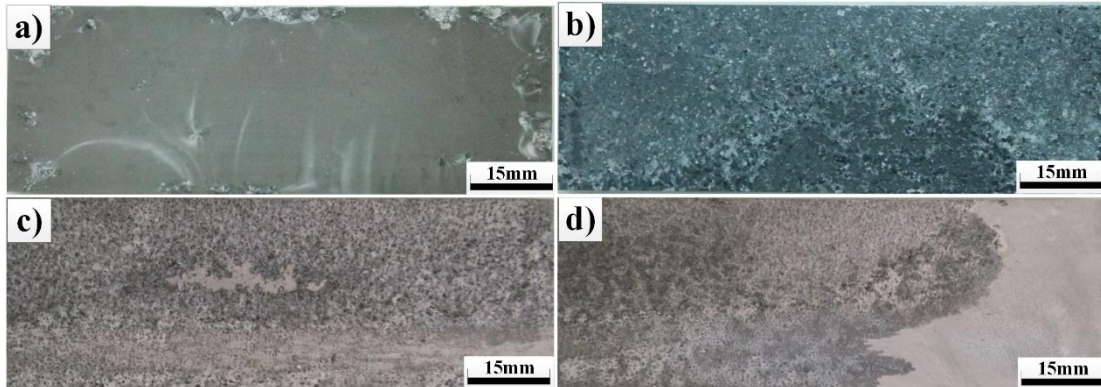


Fig. 10. Surface morphology after exfoliation corrosion of Al-4.5Zn-1.5Mg(wt.%) alloy inside the area of flame rectification after different numbers of FR in 350°C (a) base metal, (b) one time, (c) two times (d) three times

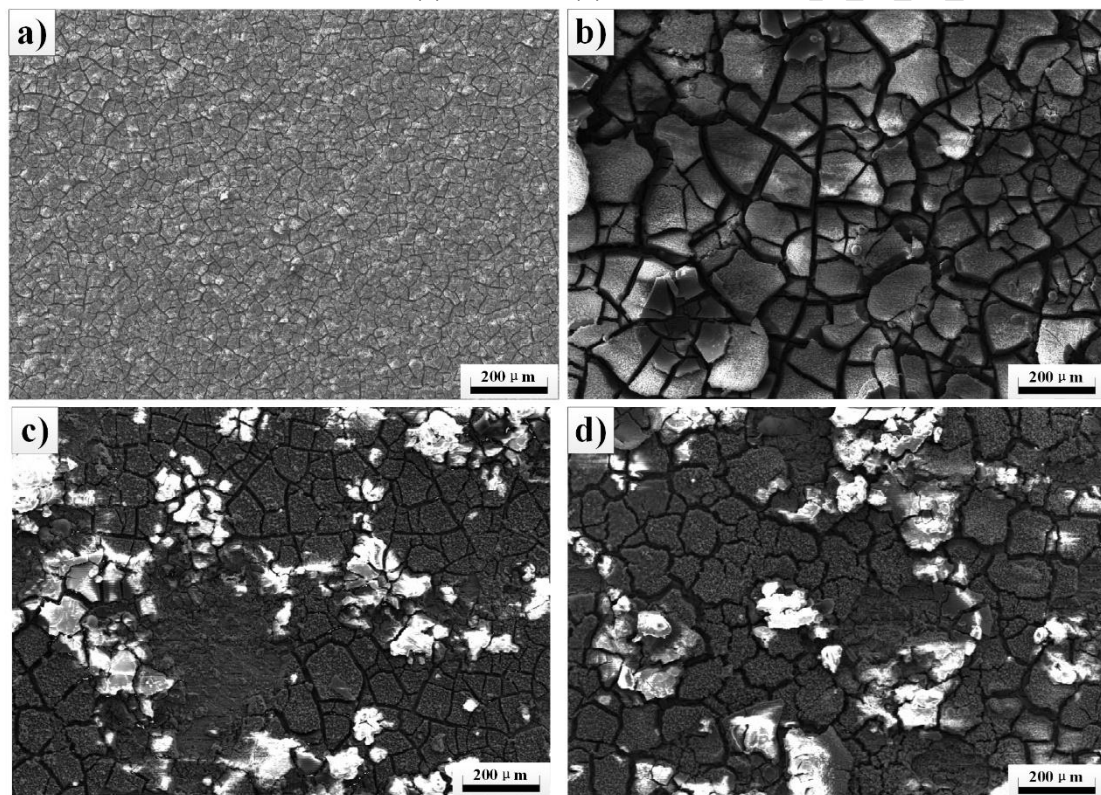


Fig. 11. SEM morphology of Al-4.5Zn-1.5Mg(wt.%) alloy after exfoliation corrosion inside the area of flame rectification after different numbers of FR in 350°C (a) base metal, (b) one time, (c) two times (d) three times

The macroscopic morphology of exfoliation corrosion of Al-4.5Zn-1.5Mg (wt.%) alloy outside the straightening area at different FR times at 350°C is shown in Fig. 12. As can be seen from the figure, the degree of corrosion of the specimens outside the straightening area is much lighter than that inside the straightening area. It exhibits a macroscopic morphology similar to that of the unstraightened, loss of metallic lustre, severe flaking at edges only. The difference between the right side of the specimen in Fig. 12(b), and the overall corrosion degree may be due to the sampling process is not standardized, so that the right side is taken to the straightening area caused by.

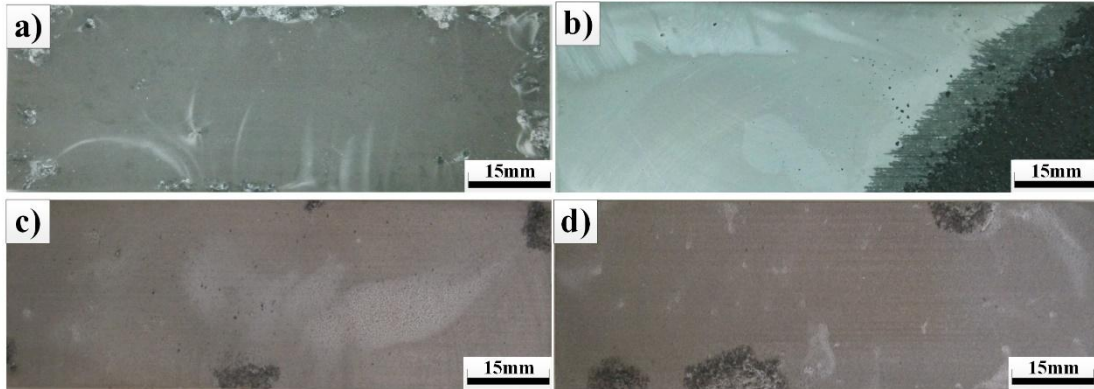


Fig. 12. Surface morphology of Al-4.5Zn-1.5Mg(wt.%) alloy after exfoliation corrosion outside the area of flame rectification after different numbers of FR in 350°C(a) base metal, (b) one time, (c) two times (d) three times

Intercepted part of the exfoliation corrosion specimen in the scanning electron microscope observation, the results are shown in Fig. 13. As can be seen from the figure, the 350°C-FR specimen exfoliation corrosion is the most serious. The surface of the specimen appeared uniform along the crystalline cracks, part of the area has appeared in the phenomenon of large pieces of metal shedding. After the second and third straightening of the specimen surface appeared uniform pits, through the enlarged morphology of Fig. 14 can be found that the corrosion pits have entered the metal surface at a certain depth. Among them, the number of corrosion products and corrosion pits of the third straightening specimens is higher than that of the second straightening. According to GB/T22639-2008, the exfoliation corrosion grades of the specimens outside the 350°C-FR areas of Al-4.5Zn-1.5Mg (wt%) alloy are EC, EB, and EB grades for the first, second, and third straightening, respectively.

The grain boundary is a typical surface defect. The atomic arrangement at the grain boundary is irregular, there are more defects, such as vacancies and dislocations, etc. The atomic diffusion rate at the grain boundary is much faster than that in the crystal, and the new phase is easy to nucleate preferentially at the grain boundary. For Al alloys, the number, size, and distribution of precipitates at grain boundaries and the width of the non-precipitated zone at grain boundaries will have an important effect on the intergranular corrosion resistance of the alloys as well as the stripping performance.

In order to analyse the reasons for the dramatic decrease in corrosion properties in the straightening area after a single FR of Al-4.5Zn-1.5Mg (wt%) alloy at 350°C. Transmission electron microscopy was used to observe the grain boundary morphology of the specimens in the unstraightened and in the area of 350°C-FR at one time, and the results are shown in Figs. 15-16. From the figure, it can be seen that the precipitated phase at the grain boundaries of the Al-4.5Zn-1.5Mg (wt%) alloy is mainly the discontinuously distributed η phase, with a size of about 100-200 nm. There were few precipitated phases at the grain boundaries of the unstraightened specimen, and their sizes were relatively large. After the first FR at 350°C, the number of precipitated phases at the grain boundaries of the specimen increased sharply, and the spacing decreased and tended to be continuously distributed, while the size became smaller. In addition to the changes in the distribution of the precipitated phases, a non-precipitation band with a width of about 50 nm was found near the grain boundaries of the specimen after one FR at 350°C, as shown in Fig. 16.

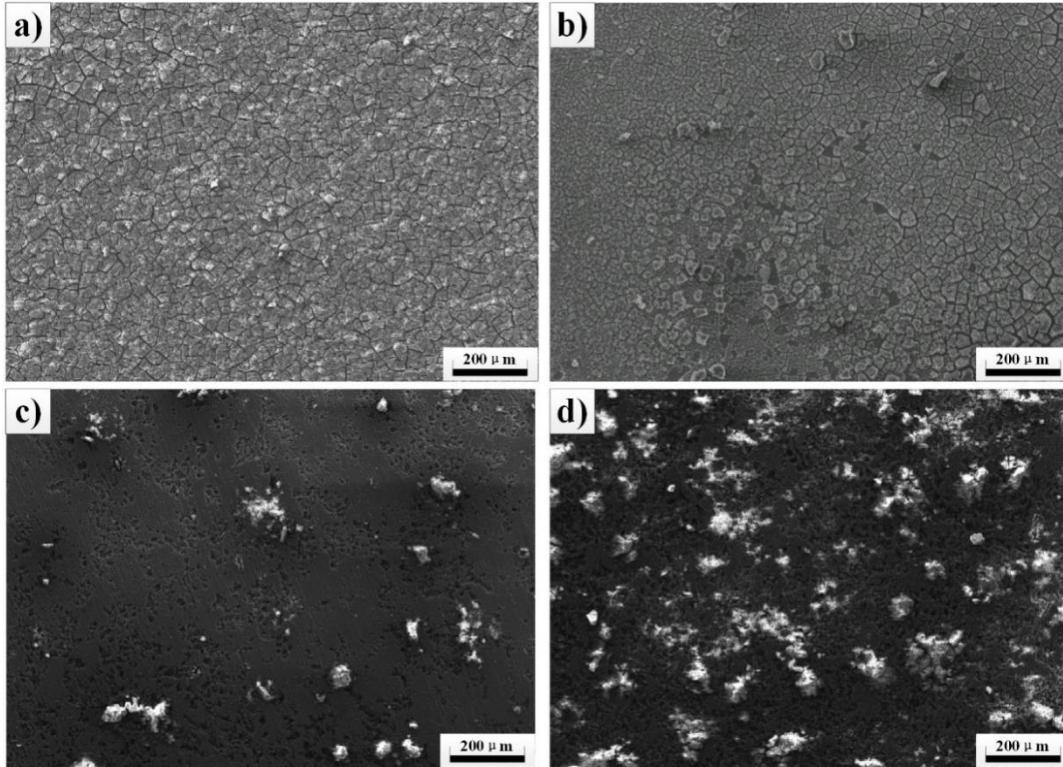


Fig. 13. SEM morphology of Al-4.5Zn-1.5Mg(wt.%) alloy after exfoliation corrosion outside the area of flame rectification after different numbers of FR in 350°C (a) base metal, (b) one time, (c) two times (d) three times

The grain boundary properties of Al-Zn-Mg alloys determine their corrosion resistance. When unstraightened, the number of precipitates on the grain boundaries is very small, being only sporadic individual particles. The potential difference between intragranular and grain boundaries is also small, which is not conducive to the formation of continuous corrosion channels. The alloy is therefore highly resistant to intergranular corrosion^[17]. The results of intergranular corrosion test show that: there is basically no reticulated grain boundaries appear, and the spalling process is often developed by intergranular corrosion, so its resistance to spalling is also relatively strong. In addition, after the 350°C-FR, the non-precipitated band appearing near the grain boundary of the specimen with a width of about 50nm can also act as an anode in the corrosive medium, thus reducing the corrosion resistance of the alloy. The formation of the non-precipitated band is associated with the solute concentration or vacancy concentration. Due to the faster desolvation at the grain boundaries, a large amount of nearby solute atoms such as Zn and Mg are consumed. This results in a lack of solute elements in the surrounding matrix and limited nucleation of precipitates. In addition, due to the lower concentration of vacancies near the grain boundaries, solute element desolvation is hindered, which also makes it difficult to precipitate the intermediate phase.

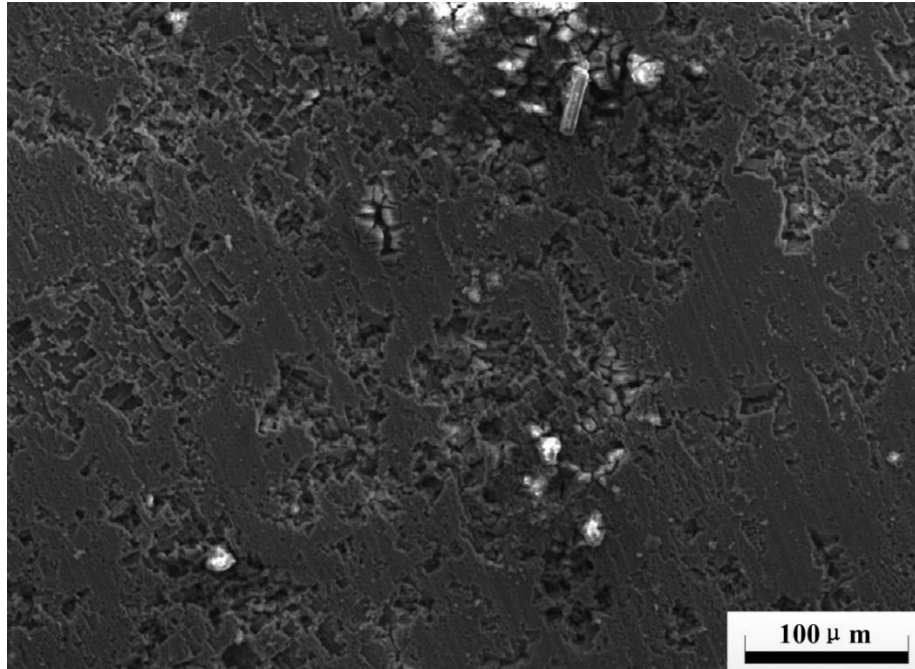


Fig. 14. Magnified morphology of Al-4.5Zn-1.5Mg(wt.%) alloy after exfoliation corrosion outside the area of flame rectification after two times of FR in 350°C

Comprehensive analysis of the above, when the FR temperature is 350°C, the second straightening is more suitable for Al-4.5Zn-1.5Mg (wt.%) alloy. Inside the straightening area, its tensile strength and elongation are higher than that of the parent material. Outside the straightening area, the tensile strength is higher than that of the parent material. The elongation decreases slightly, and the overall corrosion performance decreases to a lower degree, so the overall performance is better^[18].

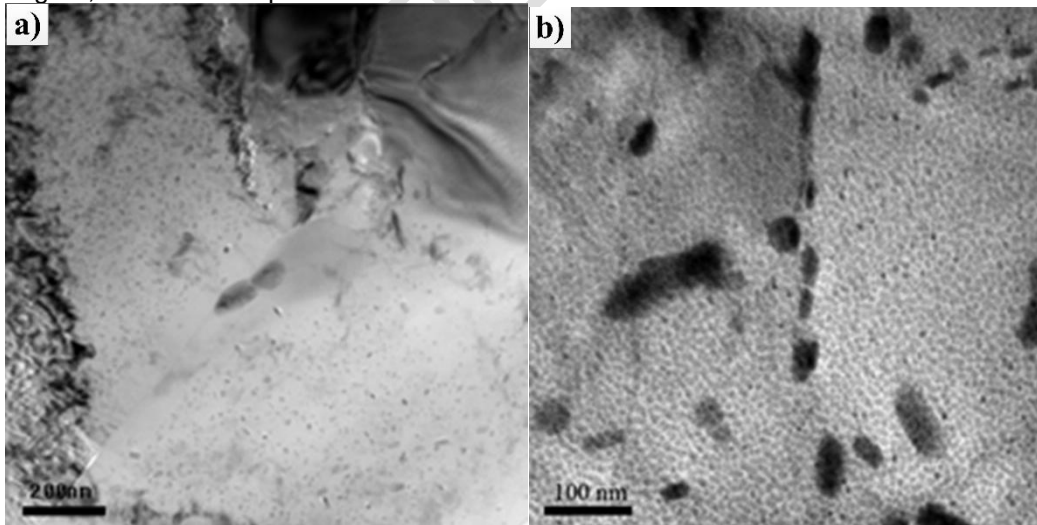


Fig. 15. TEM images of grain boundaries of Al-4.5Zn-1.5Mg(wt.%) alloy in base metal(a) and inside the area of flame rectification after one time of FR in 350°C (b)

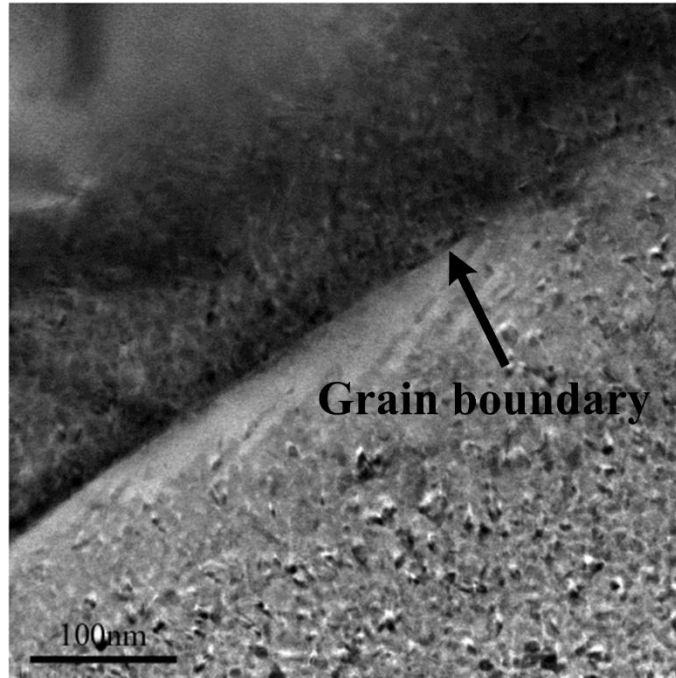


Fig. 16. Images of precipitation free zone of Al-4.5Zn-1.5Mg(wt.%) alloy inside the area of flame rectification after one time of FR in 350°C

4. CONCLUSION

The mechanical properties and corrosion performance of Al-Zn-Mg alloy through varied flame rectifications was studied based on the intergranular corrosion, exfoliation corrosion experiment. The results showed that the FR accelerated the corrosion susceptibility of Al-Zn-Mg alloy. And the maximum intergranular corrosion depth is detected with the value of 105 μ m after one time of FR. The tensile strength of Al-Zn-Mg alloy decreased to 317 MPa after one time of FR, but increased to 387 MPa after two times of FR in 350 °C. The change of corrosion resistance of Al-Zn-Mg alloy with varied FR is mainly associated with the transformation of precipitates and grains. After one time of FR, a phenomenon of "redissolution" of precipitated phases occurs. However, there is a notable increase in the precipitation of phases within the grains after two and three times of FR at 350°C. After one time of FR, small-sized new grains appear at the grain boundaries of the elongated grains within the correction area, which is the result of incomplete recrystallization in the alloy. In conclusion, when the flame temperature is 350°C, two times of FR is the most suitable for Al-Zn-Mg alloy.

REFERENCES

- [1] TT Wang, YL Wang, X Yang et al. Cracks and process control in laser powder bed fusion of Al-Zn-Mg alloy, *J. Manuf. Process.*2022;81:571-579.
- [2] Deng D. FEM prediction of welding residual stress and distortion in carbon steel considering phase transformation effects. *Mater. Des.* 2009;30:359-366.
- [3] Deng D, Murakawa H. Prediction of welding distortion and residual stress in a thin plate butt-welded joint, *Comp. Mater. Sci.* 2008;43:353-365.
- [4] Deng D, Murakawa H, Liang W. Numerical simulation of welding distortion in large structures, *Comput. Method. Appl. M.*2007;196:4613-4627.

- [5] Zhang Z, Jiang Z, Yu C. Automated flame rectification process planning system in shipbuilding based on artificial intelligence. *Int. J. Adv. Manuf. Technol.* 2006;30:1119-1125.
- [6] Lacalle R, Álvarez JA, Ferreño D, Portilla J, Ruiz E, Arroyo B, Gutiérrez-Solana F. Influence of the flame straightening process on microstructural, mechanical and fracture properties of S235 JR S460 ML and S690 QL structural steels, *Exp.Mech.* 2013;53:893-909.
- [7] Shuai Li, Honggang Dong, Peng Li, Su Chen. Effect of repetitious non-isothermal heat treatment on corrosion behavior of AlZn-Mg alloy, *Corros. Sci.* 2018;131:278-289.
- [8] Shuai Li, Microstructure, mechanical properties and corrosion behavior of Al-ZnMg alloy MIG welded joint, Dalian University of Technology, Dalian, China, 2018 D.S. Dissertation.
- [9] Jiang L, Wang Y, Liu A. Effect of flame straightening on microstructures and properties of welded joint of aluminium alloy for high-speed train, *T Mater. Heat Treat.* 2003;24:59-61.
- [10] Xiong Z. Effect mechanism of heatstraightening temperature on microstructure and properties of Aluminum alloy joint in high-speed trains. Harbin Institute of Technology, Harbin, China. M.S. Dissertation; 2014.
- [11] Avent RR. Heat-straightening of steel –Fact and fable, *J. Struct. Eng. ASCE.*1989;115:2773-2793.
- [12] Avent RR, Fadous GM. Heat-straightening prototype damaged bridge girders, *J. Struct. Eng. ASCE.* 1989; 115:1631- 1649.
- [13] Avent RR, Mukai DJ. What you should know about heat straightening repair of damaged steel. *Eng. J. AISC.* 2001; 38:27-49.
- [14] ASTM G110-92. Standard practice forevaluating intergranular corrosion resistance of heattreatable aluminum alloys by Immersion in Sodiumchloride + hydrogen peroxide solution; 2009.
- [15] ASTM G34-01. Standard test method for exfoliation corrosion susceptibility in 2xxx and 7xxx Series Aluminum Alloys (EXCO Test); 2013.
- [16] P Li, YQ Wang, S Wang et al. Corrosion behavior of refilled friction stir spot welded joint between aluminium alloy and galvanized steel, *Mater Res Express.* 2018; 5:096524.
- [17] QY Ding, YX Qin, YY Cui. Galvanic corrosion of aircraft components in atmospheric environment, *J. Chin. Soc. Corrosi. Protect,* 2020; 40(5):455–462
- [18] YT Ma, HG Dong, YQ Wang et al. Efect of Zn coating on microstructure and corrosion behavior of dissimilar joints between aluminum alloy and steel by refilled friction stir spot welding, *J. Appl. Electrochem,* 2022;52:85-102.